Alleviating hysteresis and improving device stability of perovskite solar cells via alternate voltage sweeps*

Chao Xia(夏超)[1], Wei-Dong Song(宋伟东)[1], Chong-Zhen Zhang(张崇臻)[1], Song-Yang Yuan(袁松洋)[1], Wen-Xiao Hu(胡文晓)[1], Ping Qin(秦萍)[1], Ru-Peng Wang(王汝鹏)[1], Liang-Liang Zhao(赵亮亮)[1], Xing-Fu Wang(王幸福)[1], Miao He(何苗)[1], and Shu-Ti Li(李述体)[1,2,†]

[1] *Guangdong Provincial Key Laboratory of Nanophotonic Functional Materials and Devices, Institute of Opto-electronic Materials and Technology, South China Normal University, Guangzhou* 510631, *China*

[2] *Guangdong Engineering Research Center of Optoelectronic Functional Materials and Devices, Institute of Opto-electronic Materials and Technology, Guangzhou* 510631, *China*

(Received 18 May 2016; revised manuscript received 11 September 2016; published online 8 December 2016)

The anomalous hysteresis in a perovskite solar cell induced by an asymmetric field is confirmed by a capacitance–voltage measurement. By applying several cycles of alternating reverse and forward scans, this hysteresis phenomenon is obviously alleviated, resulting in a hysteresis-less state in the perovskite solar cell. Meanwhile, the open-circuit voltage and power conversion efficiency of the perovskite solar cell are enhanced by 55.74% and 61.30%, respectively, while the current density and fill factor keep almost invariable. The operation of alleviating hysteresis is essential for further research and is likely to bring in performance gains.

Keywords: perovskite solar cells, hysteresis behavior, alternate voltage sweeps, built-in electric field

PACS: 84.60.Jt, 88.40.H−, 75.60.Ej, 94.20.Ss **DOI:** 10.1088/1674-1056/26/1/018401

1. Introduction

In the last five years, the hybrid inorganic–organic perovskite attracts lots of attention due to its great potential as a light absorber in new generation film solar cells.[1–4] Hybrid perovskites have exhibited excellent solar energy conversion efficiencies in thin film device architectures, meso-structured devices, and inverted devices.[5–7] Thanks to extensive attention and research, solar energy conversion efficiencies have dramatically soared from 3.8% to 20.1%.[8–12] However, the current is found to depend on the condition of the bias voltage applied to the device when taking photocurrent–voltage measurement, which is known as the hysteresis phenomenon.[13] Because of the present of the hysteresis phenomenon, it is difficult to correctly evaluate the performance of perovskite solar cells, i.e., some previously reported efficiencies may be overestimated.[14] The intensity of hysteresis is influenced by the device architecture, scan parameter, and pretreatment.[15–18] At the present stage, in order to obtain reliable data, a main strategy is that the efficiency is determined by holding the cell close to the maximum power point until steady-state power output is achieved.[13] Various studies have been made to reduce or eliminate the hysteresis in perovskite solar cells. Jeon *et al.* reported that a device architecture with meso-structured scaffold of titania performed hysteresis-less.[19] Seok *et al.* employed a combination of $MAPbBr_3$ and $FAPbI_3$ with a bilayer architecture to act as the light absorber, and poly(bis(4-phenyl)(2,4,6-trimethylphenyl)amine) (PTAA) to work as the hole transport layer (HTL), which successfully avoided hysteresis.[20] Moreover, Snaith *et al.* demonstrated that inserting a thin iodopentafluorobenzene film between the perovskite layer and the hole transport layer could effectively reduce the current hysteresis.[21] The physical origin of the hysteresis phenomenon is still under debate. Grätzel proposed that the displacement of the $CH_3NH_3^+$ cations caused the hysteresis phenomenon.[22] McGehee *et al.* attributed the anomalous hysteresis to the ferroelectric or photo-induced ions migration in perovskites.[23] Snaith *et al.* speculated that the charge trap under forward scan influenced the extraction of the photo-excited carrier.[24] However, accurate understanding of the origin of hysteresis is important to fully optimize the devices, and could play an important role in guidance for further improvements of photovoltaic performance and stability of solar cells.

In this study, the hysteresis behavior in a perovskite solar cell is found to be associated with the asymmetric field, according to the experimental results of capacitance–voltage measurement. We investigate the anomalous hysteresis by applying several cycles of alternating reverse and forward scans. An alleviation of hysteresis is observed after the voltage scans. The corresponding open-circuit voltage and energy conversion in the perovskite solar cell under forward scan are simultaneously enhanced. The alleviation of hysteresis under sweep

*Project supported by the National Natural Science Foundation of China (Grant Nos. 11474105 and 51172079), the Science and Technology Program of Guangdong Province, China (Grant Nos. 2015B090903078 and 2015B010105011), the Science and Technology Project of Guangzhou City, China (Grant No. 201607010246), and the Program for Changjiang Scholars and Innovative Research Team in Universities of China (Grant No. IRT13064).

†Corresponding author. E-mail: lishuti@scnu.edu.cn

© 2017 Chinese Physical Society and IOP Publishing Ltd

process is ascribed to a balance state in the perovskite solar cell caused by the voltage scanning. This is not an exhaustive study, but it is of benefit to alleviate the hysteresis and further to obtain an accurate assessment of the conversion efficiency in perovskite solar cells.

2. Experiment

2.1. Device fabrication

The devices were fabricated with the architecture of FTO/compact-TiO_2/$CH_3NH_3PbI_{3-x}Cl_x$/spiro-OMeTAD/MoO_3/Ag. The FTO (7 Ω/sq) substrates were corroded by Zn powder and HCl, and this was followed by cleaning in sequence by lotion, deionized water, acetone, and isopropanol in ultrasonic bath, and then drying at 90 °C. Our compact-TiO_2 precursor was prepared by mix of the solution with 369.00 μL titanium isopropoxide (Aladdin) dissolved in 2.53 mL isopropanol (Sigma Aldrich) and 35 μL HCl (Sinopharm Chemical Reagent Co. Ltd) dissolved in 2.53 mL isopropanol (Sigma Aldrich). After plasma treat, the compact-TiO_2 precursor was spin-coated at 6000 rpm for 45 s, and sintered at 450 °C for 50 min. For the perovskite layer, 661.6 mg $PbCl_2$ (Sigma Aldrich) and 954.00 mg MAI (Dyesol) were dissolved in 2.00 mL dimethyl (Sigma Aldrich) and the perovskite precursor solution was heated at 50 °C for 12 h. After that, the perovskite precursor was spin-coated on the compact-TiO_2 layer at 4000 rpm for 45 s. The hole transport layer (HTL) was prepared by spin coating a solution of 144.60 mg spiro-OMeTAD (Luminescence Technology Crop.) dissolved in 2.00 mL chlorobenzene (Sigma Aldrich) with the additives of bis(trifluoromethane)sulfonimide lithium salt (17.5 mL from a stock solution of 520.00 mg/mL in acetonitrile) and 29.00 mL of 4-tert-butylpyridine (Aldrich) at 4500 rpm for 30 s. The MoO_3 and argentum (Ag) electrodes were thermally deposited with thicknesses of 10 nm and 100 nm, respectively.

2.2. Device characterizations and measurements

The current–voltage (I–V) test was conducted by using Keithley 2400 source meter under illumination of AM 1.5G 100 mW/cm^2. For both reverse (1.2 V to −0.2 V) and forward (−0.2 V to 1.2 V) scans, the scan rate was maintained at 0.01 V/s during the tests. The capacitance–voltage (C–V) test was performed by using HP 4192A LF impedance analyzer. The electrodes were finished by OLED450B thermally deposited system.

3. Results and discussion

The architecture of the perovskite solar cells studied in this work was designed to be FTO/compact TiO_2/$MAPbI_xCl_{3-x}$/Spiro-OMeTAD/Ag, as depicted in Fig. 1(a). Typical current–voltage curves under forward and reverse scans are shown in Fig. 1(b). Because of the hysteresis, it is obvious that the current–voltage curve under forward scan is much lower at each voltage than that under reverse scan. In this case, the device shows a better photovoltaic characteristic under reverse scan than that under forward scan.

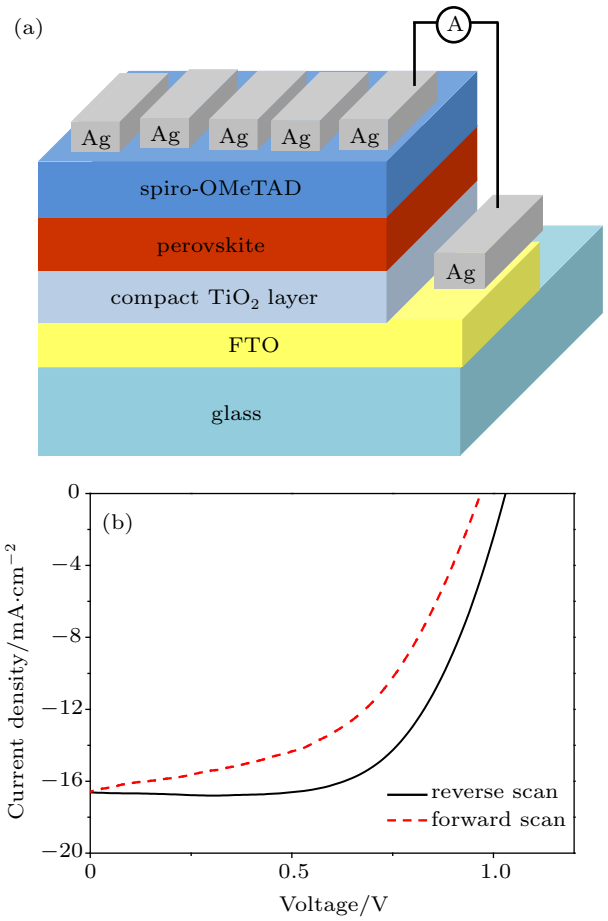


Fig. 1. (color online) (a) Schematic image of the device structure of the perovskite solar cell. (b) Current–voltage curves under forward and reverse scans, respectively.

In order to alleviate this hysteresis, the device was treated by applying repeated forward and reverse sweeps. Here, a forward scan followed by a reverse scan is defined as one scan cycle. Interestingly, as shown in Fig. 2, the I–V curves of the devices show an evolution during the subsequent several cycles of scan. Two obvious changes can be observed. First, the I–V curves under forward condition tend to be more stable than the initial one, which shows a large fluctuation. Second, in all the subsequent operation cycles, the solar cells perform better than the initial one, while the hysteresis still exists but showing an obvious relaxation in the subsequent measurement.

As illustrated in Fig. 2, for the initial test, the device has a worse photovoltaic performance with $V_{oc} = 0.61$ V, $J_{sc} = 15.88$ mA/cm^2, FF = 44.20%, and power conversion efficiency (PCE) = 4.28%. However, after seven repeated scan cycles, the device presents a significantly enhanced performance with $V_{oc} = 0.95$ V, $J_{sc} = 15.51$ mA/cm^2, FF = 48.33%,

and PCE = 6.91%. The open-circuit voltage and conversion efficiency are enhanced by 55.74% and 61.30%, respectively. In addition, the *I*–*V* curves under forward scan exhibit a little difference from those under reverse scan, indicating that the hysteresis is alleviated after the voltage sweeps. Moreover, the elimination of the zigzag-like structure in the initial *I*–*V* curve of forward scan also indicates that the device becomes more stable. Some points should be illustrated here. If the cycles of reverse and forward scan were not applied, i.e., only continuous forward sweeps, the obtained *I*–*V* curves showed little changes (see in SI). Therefore, it could be confirmed that the reduction and alleviation of hysteresis in the perovskite solar cells are induced by the voltage sweep operation.

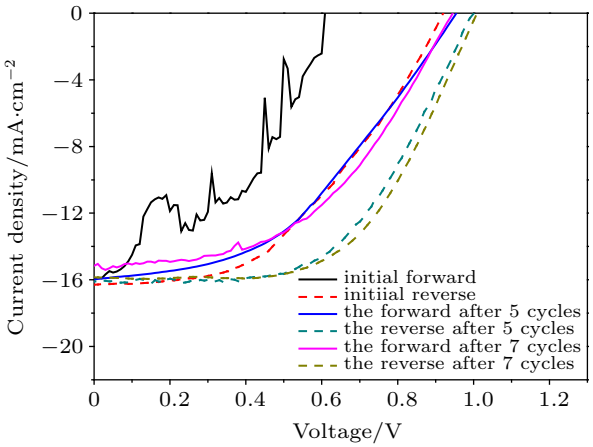


Fig. 2. (color online) Alternate voltage sweeps effects on photovoltaic performance of perovskite solar cell under illumination.

A non-dimensional hysteric index (HI) is utilized to quantify the hysteresis effect.[25] Specifically, the HI is defined as

$$\mathrm{HI} = \frac{J_{\mathrm{scan}-}(V_{\mathrm{oc}}/2) - J_{\mathrm{scan}+}(V_{\mathrm{oc}}/2)}{J_{\mathrm{scan}+}(V_{\mathrm{oc}}/2)} \times 100\%, \qquad (1)$$

where $J_{\mathrm{scan}-}(V_{\mathrm{oc}}/2)$ is the photocurrent at the bias equal to the half of the open-circuit voltage under the reverse scan, $J_{\mathrm{scan}+}(V_{\mathrm{oc}}/2)$ is the photocurrent for the forward sweep. A lower HI means less different between the forward and reverse scans, and thus less hysteresis. A HI of 0 corresponds to a cell without hysteresis. According to Eq. (1), the HIs calculated by experimental data are listed as follows. The HI in the initial cycle is 32.59%, while it decreases to 14.48% and 14.50% in the 5th and the 7th cycles, respectively. The HI index decreases and inclines to a constant value, which also elucidates that the device becomes more stable under the operation.

The capacitance effect in the PN junction of the perovskite solar cell should be the underlying inducement of the hysteresis by summarizing our results. In fact, the forward and reverse operations display great similarity with the capacity charge and discharge process in a capacitor. When the capacitor is charged (forward scan), the charges are stored into the device, and the charges prevent the current transferring through the perovskite solar cells, which results in a low open circuit voltage of 0.61 V under the initial test as demonstrated in Fig. 2. However, for the reverse scan, the follow-up operation, the charges in the device are liberated, which gives rise to a higher open circuit voltage of 0.95 V. Shi deemed that the ability of electronic transmission of the perovskite layer was influenced when a zigzag-like *I*–*V* curve appeared.[26] This anomalous inflexion is relieved as shown in the *I*–*V* curves, signifying that the electron's transmission is becoming easier in the perovskite layer. Thus, a better photovoltaic performance is exhibited in subsequent measurements.

Specifically, the evolutions of the performance parameters in all cycles are summarized in Fig. 3. The open-circuit voltage (V_{oc}), short-circuit current density (J_{sc}), fill factor (FF), and power conversion efficiency (PCE) under forward and reverse sweep during each cycle are sketched. For forward condition, as a general trend, the open-circuit voltage is enhanced greatly at the first several cycles and saturates at around 0.95 V in the subsequent cycles, as depicted in Fig. 3(a). The initial value of the open-circuit voltage soars from 0.61 V to 0.95 V, which is enhanced by 55.74%. It is remarkable that there are fewer fluctuations for the short-circuit current density and fill factor under forward scan cycles (see Figs. 3(b) and 3(c)). The values maintain around 15.50 mA/cm^2 and 45%, respectively. Under the reverse condition, the open-circuit voltage and fill factor are sostenuto increased along with the voltage scanning process, and the short-circuit current density is not influenced by this process. The evolution of the power conversion efficiency is plotted in Fig. 3(d). As a consequence, the power conversion efficiency tends to increase under the forward and reverse scans. The power conversion efficiency in the final cycle maintains at 6.92% in forward scan, and 9.38% under reverse condition.

Figure 4(a) shows the pictorial representation of overall electric fields in the perovskite solar cell device. Under illumination, a process of migration and accumulation of photo-generated charges on the interfaces of the electrodes happens under the influence of the built-in electric field. When the number of the accumulated photo-generated charges reaches a critical value, the electric field is strong enough to influence the built-in electric flied, as schematically illustrated in Fig. 4(a). Specifically, more or less accumulated charges in the electrode interfaces directly lead to lower or higher V_{oc}. And this could be explained by the follow theory. For V_{oc}, it is influenced by the effective potential barrier for charge injection at electrode interfaces when the photo-current is neutralized by the injection current. The dark injection barrier could be calculated by the following equation:

$$n_{\mathrm{i}} = N_{\mathrm{t}} \exp\left(-\frac{\phi_{\mathrm{i}}}{k_{\mathrm{B}}T}\right), \qquad (2)$$

where n_{i} represents the surface charge density, N_{t} is the volume density of molecular sites, and ϕ_{i} is the potential barrier

at the interface between the active medium and the electrode. It is obvious that a lower surface charge reflects a higher potential barrier. When the device is in the open-circuit condition, the surface charge density is constituted by the dark carriers (the carriers injected from the electrodes) and the photo-generated carriers (the carriers accumulated at the electrode interfaces). As a result, a lower accumulation of the photo-generated charge could cause a higher interfacial potential barrier, which could result in an increase of the open-circuit voltage.

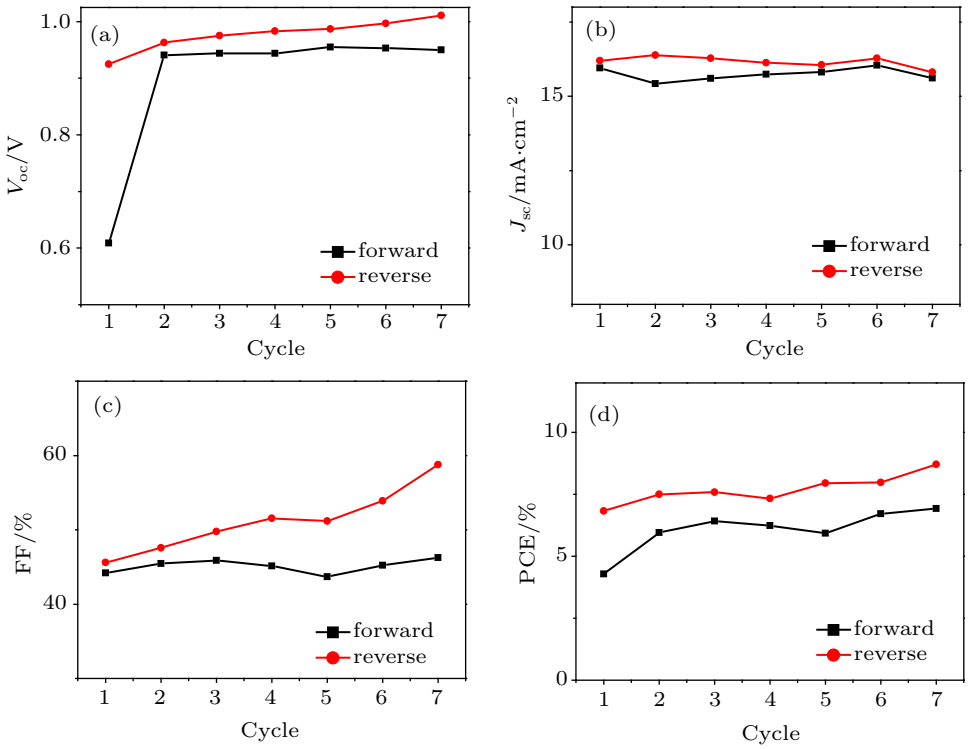


Fig. 3. (color online) (a) The open-circuit voltage (V_{oc}), (b) short-circuit current density (J_{sc}), (c) fill factor (FF), and (d) power conversion efficiency (PCE) vary with scan cycles.

In the previous studies, the capacitance–voltage (C–V) measurements were considered as an effective method for examining the surface accumulation of photo-generated charge carriers and investigating the effect of the surface charge accumulation on V_{oc}.[27,28] To confirm our results, the capacitance–voltage characteristics of our devices were tested to find out the relationship between the repeated scan cycles and the charge accumulation, as presented in Fig. 4(b). Each device was tested in sequence under the conditions of without illumination, under illumination before voltage sweep, after applying seven cycles of voltage sweep under illumination respectively, as marked in different colors in the C–V curves. The capacitance reflects the amount of charge accumulation at each electrode interface. The enhancement of capacitance from negative bias to V_{peak} indicates the increase of the surface charge accumulation; the change of bias from negative to V_{peak} provides an electric field against the built-in electric field, and thus the effective built-in electric field decreases gradually. At this beginning stage, the charges are still separated and collected by the effective built-in electric field, resulting in an increase of the capacitance, as shown by a rise tend in the curve. However, after V_{peak}, as a result of the processes of injection and recombination, a decreased trend is exhibited in the curve. As shown in Fig. 4(b), for the initial cycle with illumination, $V_{peak} = 0.55$ V is slightly lower than that under dark condition.

Additionally, the built-in electric field (E_{bt}) consists of two components: (i) the dark electric field (E_{dark}) caused mainly by the workfunction difference between the two electrodes and (ii) the electric field developed by the surface accumulation, namely, the surface accumulation-induced field (E_{ac}),[16] thus

$$E_{bt}=E_{dark}-E_{ac}. \tag{3}$$

Note that E_{ac} is an opposite field to E_{dark}. This means that lower E_{bt} and V_{peak} are caused by higher E_{ac}. A higher value of V_{peak} reflects less accumulation of charges.

The increase of V_{peak} in Fig. 4(b) reveals that our operation could reduce the carrier accumulation. According to the C–V curve, after seven cycles of sweeps under light illumination, V_{peak} and the corresponding capacitance are enhanced simultaneously.

In fact, the process of applying an external bias is equivalent to that of charge and discharge in a capacitor. Under the forward scan, the bias increases in the range from 0 to V_{peak} and the effective electric field helps to promote the charges separation and migration. Under the reverse scan, a neutraliz-

ing process happens before the bias changing to V_{peak}, therefore the accumulated charges decrease. This is consistent with our observed results that the performance is better under reverse scan. This asymmetry of the electricity field caused by the different sum of charge accumulation at each electrode under forward and reverse sweeps is the origin of the hysteresis. A reducing bias could ameliorate the field asymmetry, which could achieve an improved device performance.[29] By applying repeated and alternate sweeps, this amelioration trend is enhanced and impels the device to a balance state, a more stable inner electric field condition, thus leading to hysteresis-less and higher and more stable device performance. In additional, a recent study pointed out that under external voltage sweeps (forward and reverse), an electric field formed by ions migration in the perovskite layer might induce the hysteresis phenomenon.[30] By applying repeated and alternate sweeps, the process of ion drift trends to a balance state. This could also explain why our operation could improve the photovoltaic performance.

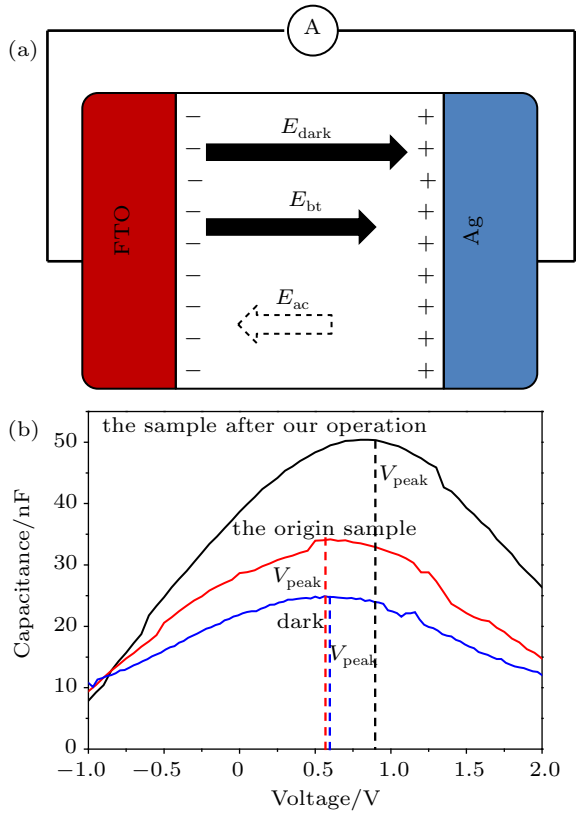


Fig. 4. (color online) (a) Schematic diagram of overall electric field in perovskite solar cells. (b) *C*–*V* characteristics for FTO/compact TiO_2/$MAPbI_xCl_{3-x}$/Spiro-OMeTAD/Ag devices under different conditions.

4. Conclusion

In summary, the hysteresis behavior in a perovskite solar cell is ascribed to the asymmetric field, which is confirmed by the capacitance–voltage measurement. The anomalous hysteresis could be alleviated by applying several cycles of alternating reverse and forward scans. The corresponding open-circuit voltage and energy conversion of the perovskite solar cell under forward scan are simultaneously enhanced. These enhancements of photovoltaic performance are ascribed to that the scan voltage impels the device to a balance state.

References

[1] Green M A, Ho-Baillie A and Snaith H J 2014 *Nat. Photon.* **8** 506
[2] Yuan Y, Xu R, Xu H T, Hong F, Xu F and Wang L J 2015 *Chin. Phys. B* **24** 116302
[3] Wang F Z, Tan Z A, Dai S Y and Li Y F 2015 *Acta Phys. Sin.* **64** 038401 (in Chinese)
[4] Yao X, Ding Y L, Zhang X D and Zhao Y 2015 *Acta Phys. Sin.* **64** 038805 (in Chinese)
[5] Cao R N, Xu F, Zhu J B, Ge S, Wang W Z, Xu H T, Xu R, Wu Y L, Ma Z Q, Hong F and Jiang Z M 2016 *Acta Phys. Sin.* **65** 188801 (in Chinese)
[6] Ma Y, Zheng L, Chung Y, Chu S, Xiao L, Chen Z, Wang S, Qu B, Gong Q, Wu Z and Hou X 2014 *Chem. Commun.* **50** 12458
[7] Heo J H, Han H J, Kim D, Ahn T K and Im S H 2015 *Energy Environ. Sci.* **8** 1602
[8] Kojima A, Teshima K, Shirai Y and Miyasaka T 2009 *J. Am. Chem. Soc.* **131** 6050
[9] Dong J, Xu X, Shi J J, Li D M, Luo Y H, Meng Q B and Chen Q 2015 *Chin. Phys. Lett.* **32** 078401
[10] Li J F, Zhao C, Zhang H, Tong J F, Zhang P, Yang C Y, Xia Y J and Fan D W 2015 *Chin. Phys. B* **25** 028402
[11] Shi J J, Dong W, Xu Y Z, Li C H, Lv S T, Zhu L F, Dong J, Luo Y H, Li D M, Meng Q B and Chen Q 2013 *Chin. Phys. Lett.* **30** 128402
[12] Yang W S, Noh J H, Jeon N J, Kim Y C, Ryu S, Seo J and Seok S 2015 *Science* **348** 1234
[13] Snaith H J, Abate A, Ball J M, Eperon G E, Leijtens T, Noel N K, Stranks S D, Wang J T, Wojciechowski K and Zhang W 2014 *J. Phys. Chem. Lett.* **5** 1511
[14] McGehee M D 2014 *Nat. Mater.* **13** 845
[15] Yang X D, Chen H, Bi E B and Han L Y 2015 *Acta Phys. Sin.* **64** 038404 (in Chinese)
[16] Zhao C, Chen B, Qiao X, Luan L, Lu K and Hu B 2015 *Adv. Energy. Mater.* **5** 1500279
[17] Shao Y, Xiao Z, Bi C, Yuan Y and Huang J 2014 *Nat. Commun.* **5** 5784
[18] Hoke E T, Slotcavage D J, Dohner E R, Bowring A R, Karunadasa H I and McGehee M D 2015 *Chem. Sci.* **6** 613
[19] Jeon N J, Noh J H, Kim Y C, Yang W S, Ryu S and Seok S 2014 *Nat. Mater.* **13** 897
[20] Jeon N J, Noh J H, Yang W S, Kim Y C, Ryu S, Seo J and Seok S 2015 *Nature* **517** 476
[21] Abate A, Saliba M, Hollman D J, Stranks S D, Wojciechowski K, Avolio R, Grancini G, Petrozza A and Snaith H J 2014 *Nano Lett.* **14** 3247
[22] Michael G 2014 *Nat. Mater.* **13** 838
[23] Unger E L, Hoke E T, Bailie C D, Nguyen W H, Bowring A R, Heumüller T, Christoforod M G and McGehee M D 2014 *Energy Environ. Sci.* **7** 3690
[24] Wojciechowski K, Stranks S D, Abate A, Sadoughi G, Sadhanala A, Kopidakis N, Rumbles G, Li C Z, Friend R H, Jen A and Snaith H J 2014 *ACS Nano* **8** 12701
[25] Sanchez R S, Gonzalez-Pedro V, Lee J W, Park N G, Kang Y S, Mora-Sero I and Bisquert J 2014 *J. Phys. Chem. Lett.* **5** 2357
[26] Shi J J, Wei H Y, Zhu L F, Xu X, Xu Y Z, Lv S T, W H J, Luo Y H, Li D M and Meng Q B 2015 *Acta Phys. Sin.* **64** 038402 (in Chinese)
[27] Zang H, Liang Y, Yu L and Hu B 2011 *Adv. Energy Mater.* **1** 923
[28] Zang H, Xu Z and Hu B 2010 *J. Phys. Chem. B.* **114** 5704
[29] Zhang Y, Liu M, Eperon G E, Leijtens T C, McMeekin D, Saliba M, Zhang W, Bastiani M, Petrozza A, Herz L M, Johnston M B, Lin H and Snaith H J 2015 *Mater. Horiz.* **2** 315
[30] Xiao Z, Yuan Y, Shao Y, Wang Q, Dong Q, Bi C, Sharma P, Gruverman A and Huang J 2015 *Nat. Mater* **14** 193